Journal of Catalysis **191,** 75–85 (2000)
doi:10.1006/jcat.1999.2772, available online at http://www.idealibrary.com on IDEAL®

Time-Resolved XAS Investigation of the Reduction/Oxidation of MoO_{3-x}

T. Ressler,*,[1] O. Timpe,* T. Neisius,† J. Find,* G. Mestl,* M. Dieterle,* and R. Schlögl*

*Department of Inorganic Chemistry, Fritz-Haber-Institut der Max-Planck-Gesellschaft, Faradayweg 4-6, D-14195 Berlin, Germany; and †European Synchrotron Radiation Facility, BP 220, 38043 Grenoble, France

Received July 22, 1999; revised November 26, 1999; accepted November 26, 1999

The bulk structure of molybdenum trioxide (MoO_{3-x}) under reductive and oxidative reaction conditions was investigated *in situ* **with time-resolved X-ray absorption spectroscopy (XAS). Alterations in the electronic and geometric structure of the molybdenum oxide systems were measured by** *in situ* **XAS at the Mo K-edge utilizing an energy-dispersive spectrometer (ESRF, ID24). Reduction and reoxidation of MoO_{3-x} at 773 K with H_2 and O_2 (100%, 1 atm), respectively, proceeded rapidly and a prompt response of the entire MoO_{3-x} bulk structure to changes in the gas composition was observed. The Mo valence of the oxidized and the reduced phase was determined to be ~6.0 and ~5.4, respectively. Principal component analysis of Mo K-near-edge (XANES) spectra of reduction—oxidation cycles identified two constituent phases, namely MoO_2 and MoO_3. No intermediate was required to describe the experimental XANES spectra, indicating a rapid transition from the MoO_3 to the MoO_2 structure without the detection of intermediates. Absorption edge fine structure analysis revealed the presence of edge-shared octahedra in the molybdenum trioxide structure presumably due to the occurrence of sheer planes. This points toward a fairly disordered MoO_{3-x} obtained from AHM which might be responsible for the observed high reaction rate. Furthermore, intriguing dynamic behavior in propene oxidation on MoO_{3-x} at 773 K was observed. Periodic oscillations were found in the Mo 1*s*–4*d* pre-edge peak. The observed dynamic behavior appears to be related to an oscillating alteration in the degree of distortion of MoO_6 octahedra. Hydrogen pulses were found to perturb the periodic oscillations with the oscillation frequency exhibiting a linear dependence on the Mo valence.**

Key Words: **catalysis; molybdenum oxide; propene oxidation; bistability; dynamic behavior; chemical oscillations; EXAFS;** *in situ*; **time-resolved; X-ray absorption spectroscopy.**

INTRODUCTION

Mixed molybdenum oxide catalysts are used extensively in the selective oxidation of hydrocarbons (1, 2) and contribute significantly to the gross amount of chemicals produced by catalytic processes. Although molybdenum trioxide or molybdenum suboxides (Mo_nO_{3n-1}) possess an inferior catalytic activity, they also have been subjects of numerous studies (3), since they constitute suitable model systems to elucidate correlations between structural properties and catalytic performance. To date open questions remain regarding the Mo valence of catalytically active species (e.g., pentavalent Mo), participation of oxide ions from the catalyst bulk in the reaction (e.g., Mars–van Krevelen mechanism (4)), or the type and number of defects in the structure (e.g., crystallographic sheer planes (5)).

Temperature-programmed reduction (TPR) of bulk MoO_3 and MoO_2 have been studied in detail in the past (6, 7, and references therein). Arnoldy *et al.* postulated a two-step reduction mechanism ($MoO_3 \rightarrow MoO_2 \rightarrow Mo$). Moreover, the authors reported a strong dependence of the TPR pattern of MoO_3 on water content of the reducing mixture, sample size, precalcination temperature, and heating rate, with onset temperatures of MoO_3 reduction ranging from 650 to 800 K (6). Regalbuto *et al.* studied TPR of diluted (SiO_2) and supported MoO_3 and found a considerable shift toward lower reduction temperatures for diluted MoO_3 compared to "bulk" MoO_3. The authors concluded that diluted samples undergo a low temperature autocatalytic reduction mechanism by virtue of a more efficient removal of water vapor (7). However, in the cited TPR investigations no *in situ* structural analysis of the systems studied or dependence of reducibility on structural defects was provided.

In two recent investigations of molybdenum oxides in catalysis, conclusions regarding active species or reaction mechanisms were drawn from *ex situ* experiments. Aritani *et al.* (8) studied binary Mo–Mg oxides by *ex situ* Mo and Mg K-edge X-ray adsorption fine structure (XAFS) experiments. The authors found that a Mo enriched binary oxide is readily reduced with H_2 at 773 K to form a MoO_2 phase not detectable with XRD. It was concluded that this phase contains highly dispersed low valent Mo ions that work as active center for propene metathesis. Unfortunately, no *in situ* work that would yield direct evidence for this assumption is presented. Han *et al.* (9) reported a correlation of particle size and catalytic activity and selectivity for bismuth molybdate catalysts that would confirm a Mars–van

[1] To whom correspondence should be addressed. Fax: (+49) 30 8413 4405. E-mail: ressler@fhi-berlin.mpg.de.

0021-9517/00 $35.00

Krevelen mechanism for the propene oxidation on these systems. The authors deduced that a certain particle size is required to provide sufficient lattice oxide ions during the catalytic redox cycle. However, only few structural details about the catalysts are provided and no *in situ* experiments were performed.

The long-term objective of our current research effort is to reveal a correlation of bulk structural properties with catalytic performance for selective oxidation reactions on metal oxides. Therefore, we focus mainly on *in situ* investigations capable of providing experimental evidence that correlate the bulk structure of metal oxides to their catalytic reactivity and selectivity. Molybdenum oxides and sub oxides serve as model systems used to gain a better understanding of the more complex mixed oxides or heteropolyacids.

To date only a few experimental methods can be utilized to reveal structural information of dispersed and/or disordered heterogeneous catalysts *in situ* under "real" reaction conditions (high T and p) with even fewer methods suitable for dynamic studies. In this work we present first results obtained from *in situ* measurements of molybdenum trioxide under reducing and oxidizing reaction conditions using time-resolved X-ray absorption spectroscopy (TR-XAS). Element specificity and no long-range order requirements combined with the superior time-resolution of the energy-dispersive experimental configuration enables one to follow bulk structural alterations of molybdenum oxide systems under rapidly changing reaction conditions.

EXPERIMENTAL

Sample Preparation and in Situ Measurements

Molybdenum trioxide (denoted MoO_{3-x} in the following) was prepared *in situ* by thermal decomposition of ammonium heptamolybdate (AHM), $(NH_4)_6Mo_7O_{24} \cdot 4H_2O$ (Merck Co.), in He (RT–720 K, heating rate 3 K/min), followed by oxidation in air at 720 K for about 15 min. For comparison commercially available MoO_2 (Aldrich Co.) and α-MoO_3 (Merck Co.) were measured as purchased. Phase purity of the commercial compounds was verified with XRD.

For *in situ* experiments molybdenum oxides and their precursors were mixed with boron nitride (ratio 1 : 2) and 30 mg of the mixture was pressed with a force of 1 ton into a 5-mm-diameter self-supporting pellet. The absorption jump, $\Delta\mu x$, at the Mo K-edge was $\sim$1.5. *In situ* XAS experiments were carried out in a flow-reactor at atmospheric pressure. Reaction temperature and reactant mass flows were controlled with an Eurotherm PID temperature controller and Bronkhorst mass flow controller, respectively (10 ml/min He during AHM decomposition, 10 ml/min air during oxidation cycles, 10 ml/min H_2 during reduction cycles). The product composition at the *in situ* cell gas outlet was continuously monitored using a mass spectrometer in a mass scan mode (QMS200 from Balzers) with a time resolution of about 12 s per spectrum. The small cell volume (3.8 ml) allows a rapid response in the mass spectra to changes in the reaction gas composition. A setup like this is necessary for catalysis studies that aim at elucidating the correlation of bulk structural features with changes in reactant composition (e.g., catalytic activity or selectivity) (10). X-ray diffraction measurements for phase analysis were conducted at a STOE transmission diffractometer STADI-P (Ge primary monochromator, Cu$K_{\alpha 1}$ radiation) equipped with a position sensitive detector. Crystalline phase identification based on XRD patterns was aided by the ICDD-PDF-2 database.

Energy-Dispersive XAFS

XAS experiments were carried out at the Mo K-edge (19.999 keV (11)) utilizing an energy-dispersive spectrometer (European Synchrotron Radiation Facility, ESRF, ID24 (12)) equipped with a curved Si(111) polychromator in transmission mode (13). The storage ring operated at 6.0 GeV with injection currents of 200 mA in a 2/3 filling mode. In contrast to a conventional double crystal monochromator, where the photon energy is scanned stepwise by changing the Bragg angle of both crystals, the dispersive spectrometer applies a bent polychromator crystal. The sample is placed in the focal point of the polychromator, and due to the fixed energy–position correlation in the diffracted energy band, a complete absorption spectrum can be obtained by measuring the intensity distribution on a position-sensitive detector. A measuring time per absorption spectrum in the millisecond range is feasible at most currently available dispersive spectrometers.

EXAFS Data Analysis

Details on data reduction procedures for energy-dispersive X-ray absorption spectra (i.e., energy calibration, etc.) can be found in Refs. 14 and 15. XAFS analysis was carried out using the software package WinXAS97 v1.3 (16) following recommended procedures from the literature (17). Pre-edge background subtraction and normalization was performed by fitting linear polynomials to the pre-edge and the postedge region of an absorption spectrum, respectively. A smooth atomic background, $\mu_0(k)$, was obtained using a cubic spline refinement procedure. Care was taken to ensure that no contribution from the first oxygen shell is removed from the experimental signal. Fitting range in k space, number of splines, and k weighting were optimized to afford a rigid background curve at low k and minimization of low R peaks in the Fourier transformed signal. The radial distribution function FT($\chi(k)$) was obtained by Fourier transforming the k^3-weighted experimental

extended fine structure (EXAFS) $\chi(k)$, multiplied by a Bessel window, into the R space.

Calculation of theoretical EXAFS spectra and refinement to experimental data was carried out using theoretical backscattering phases and amplitudes obtained from the ab initio multiple-scattering code FEFF 7 (18). Parameters that are determined by a least-squares fit of the standard EXAFS formula (19) to experimental spectra are S_0^2, the passive electron reduction factor (20), R_j, the inter atomic distance, and σ_j^2, the relative mean square displacement about the equilibrium bond length of the jth scattering paths (Debye–Waller factor). Coordination numbers (CN) were kept invariable in the refinement. EXAFS refinements reported in this work were carried out in R space to magnitude and imaginary part of a Fourier transformed k^3-weighted experimental $\chi(k)$. Further details on the EXAFS refinement procedure employed can be obtained from the cited literature (21).

RESULTS

Dispersive EXAFS Data Evaluation

With the energy-dispersive setup employed here (Si(111) at 20.0 keV) an energy range of more than 1.0 keV ($k \approx 16$ Å^{-1}) is diffracted by the bent polychromator. However, spurious structure and peaks due to multiple-scattering effects in the polychromator (so-called "glitches") distort the EXAFS $\chi(k)$ and renders the signal at $k > 14.0$ Å^{-1} unusable for EXAFS analysis. Therefore, in the work described here the experimental $\chi(k)$ is extracted only up to $k = 14.0$ Å^{-1}. Figure 1 shows an experimental $\chi(k)$[2.0–14.0 Å^{-1}] of MoO_2 measured in 30 s.

Since the usability of energy-dispersive EXAFS data for structural investigations is still subject to debate, we attempted to evaluate the validity of a detailed EXAFS analysis of energy-dispersive data. Therefore, an experimental $\chi(k)$ of MoO_2 (Fig. 1) was compared to theoretical EXAFS functions of MoO_2 based on two slightly different

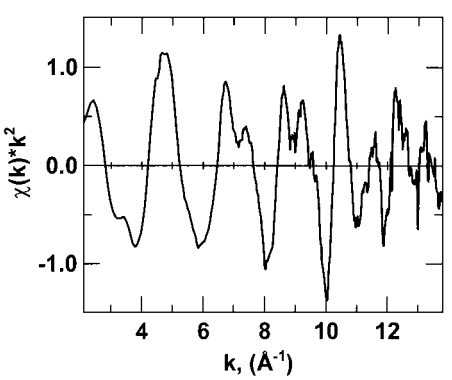

FIG. 1. Experimental $\chi(k)$ of molybdenum dioxide measured in the energy-dispersive mode in 30 s.

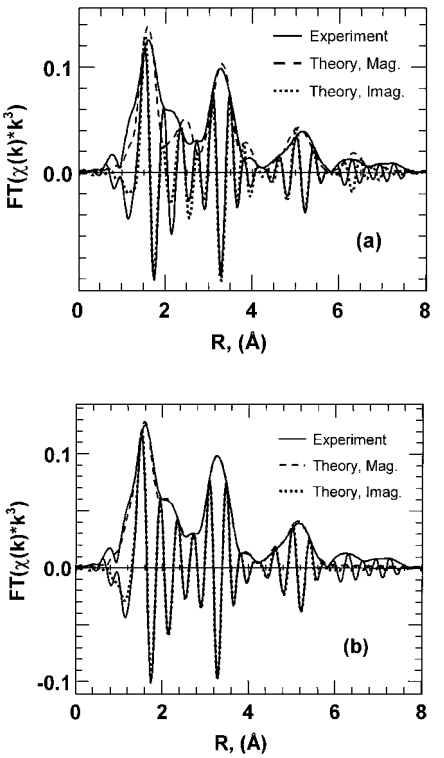

FIG. 2. Experimental and theoretical Fourier transformed $\chi(k)$ of MoO_2. Theoretical phases and amplitudes calculated for (a) a tetragonal and (b) a monoclinic MoO_2 structure were used in the refinement.

crystallographic models: (i) a tetragonal MoO_2 structure (22) ($P42/mnm$, $a = 4.86$ Å, $c = 2.79$ Å) and (ii) a monoclinic MoO_2 structure (23) ($P21/c$, $a = 5.610$ Å, $b = 4.857$ Å, $c = 5.626$ Å, $\beta = 120.9°$). The reduction in symmetry from the tetragonal to the monoclinic structure results in a splitting of coordination shell distances in monoclinic MoO_2 (Table 1).

Figure 2 depicts the FT($\chi(k)$) of MoO_2 together with theoretical XAFS functions utilizing phases and amplitudes calculated for (a) a tetragonal MoO_2 structure ($P42/mnm$, fit range 1.0–6.0 Å, 14 single scattering (SS) paths, and 23 multiple-scattering (MS) paths) and (b) a monoclinic MoO_2 structure ($P21/c$, fit range 1.0–6.0 Å, 31 SS paths and 24 MS paths). Evidently, phase (FT imaginary part, i.e., shell distances) and amplitude (FT magnitude, i.e., coordination numbers) of the tetragonal model system do not match the experimental EXAFS function of MoO_2. On the other hand, the calculated EXAFS function of the monoclinic model results in a good fit to the experimental $\chi(k)$ in both phase and amplitude (Fig. 2b). Resulting coordination shell distances of the first five shells are given in Table 1 with the refined distances deviating by less than 0.03 Å from the known crystallographic values. This excellent agreement between experiment and theory clearly confirms that energy-dispersive XAFS data can be properly calibrated and indeed can be utilized for accurate short- to

TABLE 1

Coordination Numbers (CN) and Distances (R) of Subsequent Coordination Shells around a Mo Absorber in a Tetragonal MoO_2 Structure (22) ($P42/mnm$, $a = 4.86$ Å, $c = 2.79$ Å) and a Monoclinic MoO_2 Model Structure (23) ($P21/C$, $a = 5.610$ Å, $b = 4.857$ Å, $c = 5.626$ Å, $\beta = 120.9°$) Compared to Fit Results Obtained from a Refinement of the Monoclinic Structure to an Experimental MoO_2 FT($\chi(k)$) (Fig. 2b) (Amplitude Weight Filter = 3%, 31 SS Paths, and, 24 MS Paths, Goodness of Fit = 4.9%)

	Tetragonal MoO_2		Monoclinic MoO_2		EXAFS fit	
Shell/Pair	CN	R (Å)	CN	R (Å)	CN_{Fixed}	R_{Fitted} (Å)
1st shell	4	1,959	2	1.972	2	1.934
Mo–O			2	1.986	2	2.020
	2	2,062	2	2.073	2	2.041
2nd shell	2	2,790	1	2.513	1	2.519
Mo–Mo			1	3.109	1	3.133
3rd shell	8	3,709	2	3.668	2	3.664
Mo–Mo			2	3.697	2	3.716
			2	3.703	2	3.716
			2	3.766	2	3.772
4th shell	4	4,860	1	4,670	1	4.631
Mo–Mo			2	4,857	2	4.827
			1	5,006	1	4.997
5th shell	8	5,415	2	5,155	2	5.152
Mo–Mo			2	5,359	2	5.336
			1	5,402	1	5.414
			2	5,426	2	5.414
			1	5,535	1	5.562

Note. Estimated error in R is <0.03 Å.

medium-range structure determination. In combination with an excellent time resolution and a sufficient k range at metal absorption edges higher than 12.0 keV, these capabilities shall be utilized in future investigations.

Near-Edge Structure (XANES)

Reduction or reoxidation experiments with hydrogen or oxygen utilizing MoO_{3-x} obtained from a thermal decomposition of $(NH_4)_6Mo_7O_{24} \cdot 4H_2O$ (AHM) were performed and changes in the MoO_{3-x} bulk structure were monitored with *in situ* XAS. Reactant (H_2 or O_2) flow was controlled at 10 ml/min with mass flow controllers and flow was switched from oxygen to hydrogen manually with an intervening helium purge. Owing to the small *in situ* cell volume switching between reactants results in a rapid introduction and depletion of reactants. This procedure results in what is denoted as a "pulse." Each pulse consists of a rapid increase of reactant concentration to 100%, maintained for 2.5 or 5 min (H_2 or O_2, respectively), and followed by a rapid decrease in reactant concentration as the flow is switched to He. Figure 3 shows Mo K-near-edge (XANES) spectra measured during a series of H_2 and O_2 pulses at 773 K and over a period of 50 min with a time resolution of 15 s/spectrum. Each increase or decrease in the Mo K-edge whiteline height corresponds to a H_2 or O_2 pulse, respectively, and indicates a reduction or oxidation of molybdenum. The Mo K-edge absorption threshold was determined from the first root in the first derivative of the XANES (in the following edge shifts are reported relative to the first inflection point in the Mo metal K-edge XANES at 19999 eV). The reduction or reoxidation of MoO_{3-x} also causes a shift in the Mo K-absorption edge to lower or higher photon energies, respectively, and Fig. 4 depicts Mo K-edge-shift data corresponding to absorption spectra in Fig. 3, together with the normalized mass spectrometer signal for H_2 and O_2. It can be seen from Fig. 4 that reduction and reoxidation of Mo oxide proceeded rapidly under the conditions employed (here, *rapid* refers to solid state reaction rates that are in the same order as those of the gas phase transport (subminute), in contrast to a *slow* reduction in the order of hours as previously reported (24–26)).

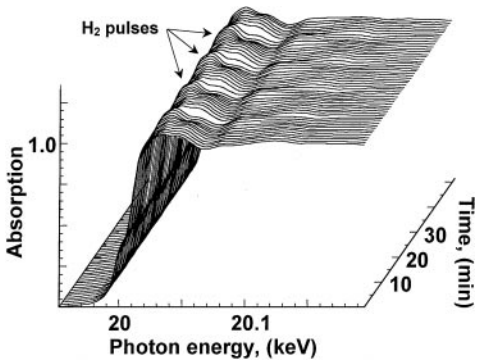

FIG. 3. Evolution of Mo K-edge XANES of MoO_{3-x} during several reduction and oxidation cycles with H_2 and O_2, respectively. A decrease in the white line indicates an increase in the Mo valence.

In addition to information on average valence and coordination geometry, the near-edge region (XANES) can be

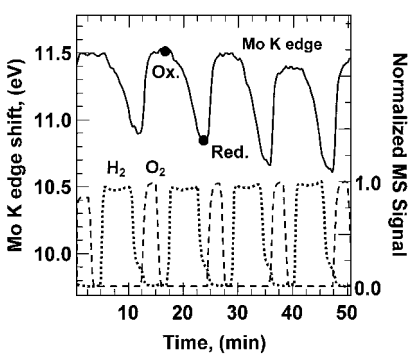

FIG. 4. Mo K-edge position (relative to the first inflection point in the Mo metal K edge XANES at 19999 eV) of MoO_{3-x} during reduction and oxidation obtained from corresponding XANES spectra in Fig. 3. Oxidized and reduced state of Mo is indicated. Normalized O_2 and H_2 MS signals are shown. A rapid response of the entire bulk sample to changes in the gas composition can be seen.

utilized to extract qualitative and quantitative information regarding the occurrence of different phases in a set of samples. In order to identify Mo oxide phases present during the reduction and reoxidation of MoO_{3-x}, principal component analysis (PCA) was employed. PCA makes use of the fingerprint characteristics of the XANES region of different phases to distinguish them in a number of spectra from mixed-phase systems. Hence, XANES analysis can afford information on low concentration or disordered systems not readily available with XRD. In addition, given a set of spectra of suitable reference compounds, PCA in combination with "Target transformation" can be utilized to identify those references that constitute probable components in the original set of XANES spectra. Details on PCA analysis and the numerical procedures employed can be obtained from the literature (27, 28). Subsequently, based on the obtained PCA results in terms of number and probable type of constituent (reference) phases, a least-squares fitting procedure can be applied to determine the amount of each phase under oxidation/reduction conditions as a function of time.

Principal component analysis of Mo *K*-edge XANES spectra of one reduction–oxidation cycle identified two constituent components to be sufficient to reconstruct the experimental XANES data. Hence, all XANES spectra of one reduction/oxidation cycle can be described by a linear combination of two Mo oxide phases within the experimental noise. Utilizing target transformation, MoO_3 and MoO_2 were identified as probable constituent phases in one reduction–oxidation cycle. The analysis of subsequent cycles yielded the same result. A least-squares fit of MoO_2 and MoO_3 reference spectra to the XANES data was used to quantify the two phases in the molybdenum oxide systems under reduction/oxidation conditions. A linear-combination XANES fit for a selected MoO_{3-x} spectrum is shown in Fig. 5, indicating the good agreement of the employed two-component fit and the experimental data. Phase analysis of one reduction/oxidation cycle is displayed in Fig. 6. Evidently, reduction with H_2 under the conditions

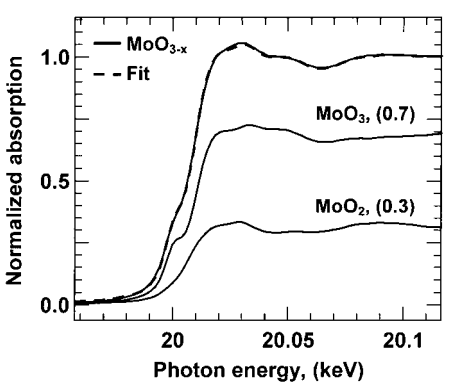

FIG. 5. Linear combination XANES fit to a selected MoO_{3-x} spectrum of Fig. 3 utilizing MoO_3 and MoO_2 reference XANES spectra.

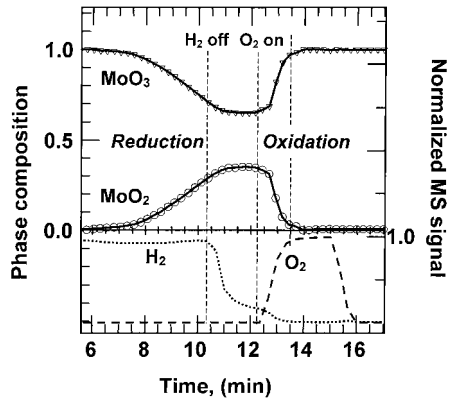

FIG. 6. Phase composition of the molybdenum oxide system in Fig. 4 during one reduction and oxidation cycle. Phase concentration was obtained from a refinement of MoO_2 and MoO_3 references spectra to each *in situ* spectrum. Dashed vertical lines indicate H_2 flow off and O_2 flow on.

employed (773 K, 4 min in 100% hydrogen) results not in complete reduction to MoO_2 but in a 1:2 mixture of MoO_2 and MoO_3. A complete reduction of MoO_3 to MoO_2 can be observed after ~8 min under the conditions employed. However, in order to avoid further reduction to Mo metal, not desirable for the experiments described here, a hydrogen pulse duration of 5 min was chosen. The average valence calculated from the concentrations of MoO_3 and MoO_2 using PCA is in agreement with the average valence (~5.4) obtained from the K-edge-shift calibration curve in Fig. 7.

Extended Fine Structure (EXAFS)

Figure 8 shows diffraction patterns for as-purchased MoO_3 and for MoO_{3-x}, obtained from a similar thermal treatment of AHM as described above and measured *in situ* at 773 K (details on the setup employed have been

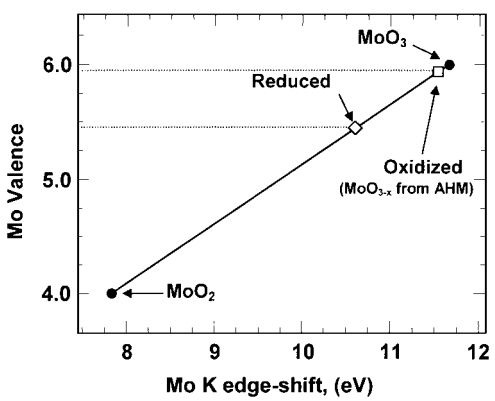

FIG. 7. Linear relationship of average Mo valence and Mo K-edge position (relative to Mo metal at 19.999 keV) calculated from K-edge position of MoO_2 and MoO_3. The linear curve is used to determine the average Mo valence of the *reduced* and *oxidized* state in Fig. 4.

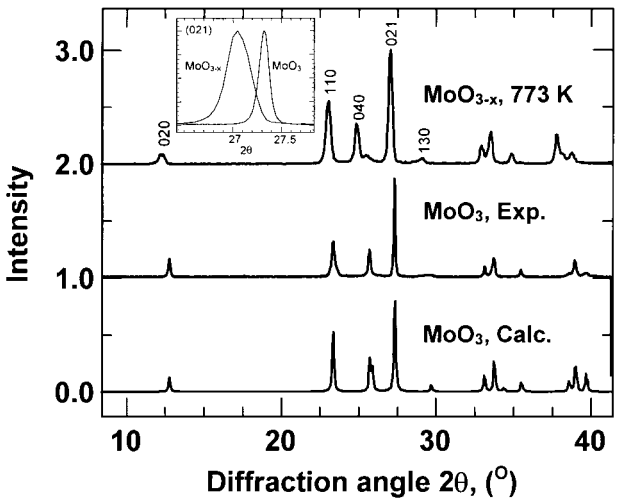

FIG. 8. X-ray diffraction patterns of as-purchased α-MoO_3, and MoO_{3-x} obtained from thermal decomposition of $(NH_4)_6Mo_7O_{24}\cdot 4H_2O$ (AHM) compared to a calculated MoO_3 pattern.

reported elsewhere (29)). The X-ray diffraction patterns of MoO_3 (as-purchased and obtained from AHM) could be indexed sufficiently with the orthorhombic structure (30) of α-MoO_3. Lattice constant refinement yielded a unit cell in good agreement with literature data (SG: *Pbmn*, $a = 3.964$ Å, $b = 13.863$ Å, $c = 3.699$ Å). A calculated XRD pattern for orthorhombic α-MoO_3 is displayed in Fig. 8.

Figure 9 displays Fourier transformed EXAFS functions of (i) as-purchased MoO_3 (at room temperature), (ii) MoO_{3-x} obtained from AHM decomposition (at 773 K, Ox. in Fig. 4), (iii) the reduced phase from Fig. 4 (at 773 K, mixture of MoO_3 and MoO_2), and (iv) MoO_2 (at room temperature). A theoretical FT($\chi(k)$) calculated for an orthorhombic α-MoO_3 structure (30) is also shown. Obvious differences in Mo_I/Mo_{II} contribution in room temperature spectra and spectra measured at 773 K (Fig. 9) are due to a temperature effect. A schematic representation of the layered α-MoO_3 structure is depicted in Fig. 10. MoO_6 octahedra in the structure are heavily distorted, resulting in Mo–O distances ranging from 1.67 to 2.33 Å. Two prominent Mo–Mo distances at 3.438 and 3.696 Å are also indicated. In agreement with XRD results, the EXAFS of as-purchased MoO_3 can very well be simulated with an orthorhombic model structure. The EXAFS function of MoO_{3-x} prepared *in situ* from AHM, however, exhibits significant differences compared to as-purchased MoO_3. Most remarkable, an additional FT peak at ~2.6 Å is apparent in the Fourier transformed $\chi(k)$. This peak is due to a short Mo–Mo distance across the edge of two neighboring MoO_6 units. Thus, in contrast to α-MoO_3, edge-shared MoO_6 octahedra appear to be present in the structure of MoO_{3-x} obtained from a thermal decomposition of AHM. For the reduced phase from Fig. 4 an increase in the second oxygen peak in the FT($\chi(k)$) indicates a decrease in octahedron distortion upon reduction and is consistent with an increased contribution of a MoO_2 phase in the Mo oxide system (Fig. 6). In addition, an alteration in the first Mo–Mo peak height (edge-shared) points toward a decreasing ratio of edge-shared to corner-shared octahedra.

Dynamic Studies

The periodic oscillations observed in time-resolved Mo *K*-edge data of MoO_{3-x} under propene atmosphere point toward an intriguing dynamic behavior of the propene oxidation at 773 K. Time-resolved XANES spectra (3 s/spectrum) of MoO_{3-x} (obtained from AHM) were collected for a period of 15 min while the Mo oxide was kept under propene atmosphere at 773 K (propene flow of 5 ml/min, no oxygen added). The XANES spectra of MoO_{3-x} under reaction conditions resembled the near-edge spectrum of as-purchased MoO_3; however, a detailed XANES analysis revealed periodic oscillations in the Mo 1*s*–4*d* pre-edge peak. Pre-edge peak height as a function of time was

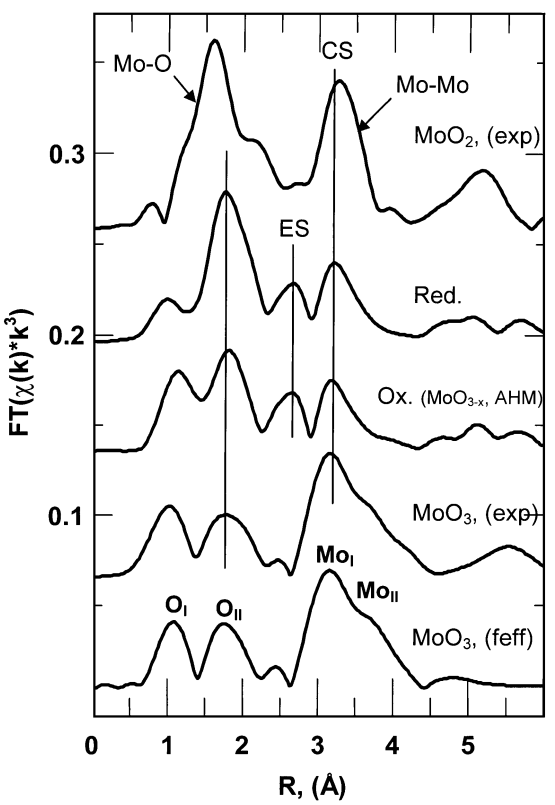

FIG. 9. Fourier transformed $\chi(k)$ of the oxidized (Ox., MoO_{3-x} obtained from AHM) and reduced state (Red.) in Fig. 4 (both at 773 K) together with XAFS $\chi(k)$ of MoO_2, and as-purchased MoO_3 (exp, both at room temperature). A theoretical MoO_3 $\chi(k)$ based on the orthorhombic α-MoO_3 (feff) structure is shown for comparison. FT peaks below 2.0 Å belong to Mo–O coordination shells. FT peaks that correspond to Mo–Mo scattering paths via MoO_6 octahedron edges (ES) or corners (CS) are indicated.

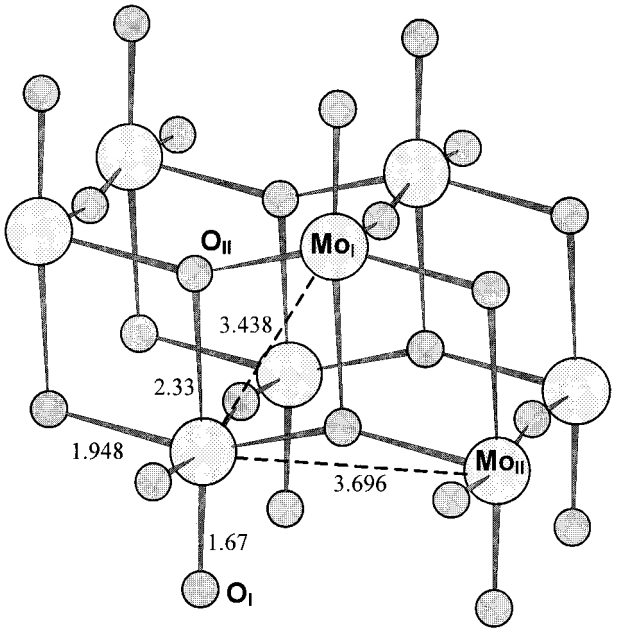

FIG. 10. Schematic representation of the orthorhombic α-MoO_3 structure (*Pbnm*, $a = 3.963$ Å, $b = 13.855$ Å, $c = 3.696$ Å (30)). Mo–O distances within a distorted octahedral coordination and two prominent Mo–Mo distances are indicated.

obtained by fitting a Gaussian profile function and an arctangent step function (Fig. 11) to the time-resolved Mo K-near-edge data. Evolution of the Mo 1*s*–4*d* pre-edge peak height under reaction conditions is shown in Fig. 12. Hydrogen pulses (5 ml/min H_2, added to the propene flow for 1 min) were found to perturb the periodic oscillations as can be seen from the more irregular behavior observable after each H_2 pulse in Fig. 12.

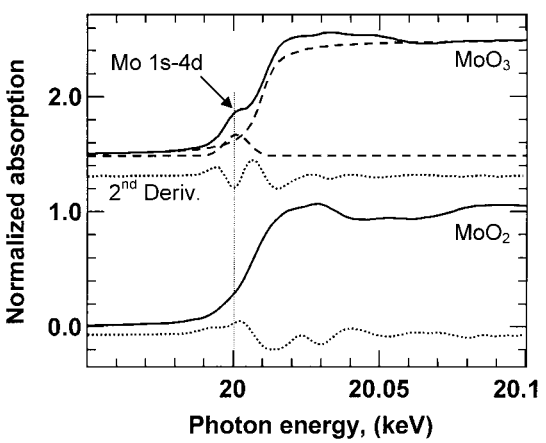

FIG. 11. Mo K-near-edge spectra of MoO_3 and MoO_2. The second derivative is shown to emphasize a pre-edge peak that corresponds to an allowed 1*s*–4*d* transition in Mo in a distorted octahedral environment. A profile refinement(Gaussian peak and arctangent step function) is displayed for MoO_3.

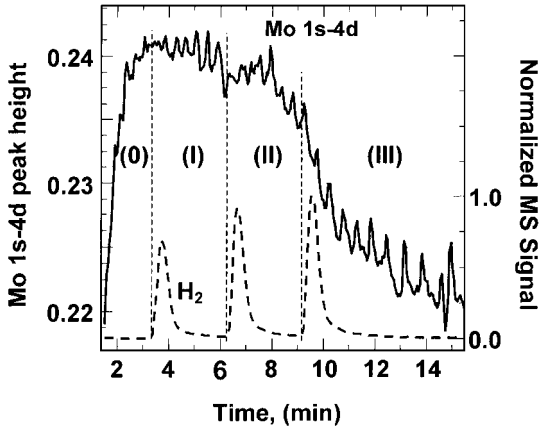

FIG. 12. Periodic behavior of the Mo 1*s*–4*d* pre-edge peak height in XANES spectra of MoO_{3-x} in a propene atmosphere at 773 K (regions I–III, constant flow of 5 ml/min, no oxygen added). In region (0) previously reduced MoO_{3-x} was reoxidized with O_2 (off at 3 min). H_2 pulses (1 min at 5 ml/min added to the propene flow) can be seen to perturb the periodic oscillations and to alter the frequency.

DISCUSSION

XANES: Mo Valence and Phase Analysis

The observed reaction rates of MoO_3 reduction and reoxidation (Fig. 4) are in contrast to results published by Carpenter *et al.* (31) who postulated a slow reduction of MoO_3 to MoO_2. Interestingly, oxidation and reduction exhibit different reaction rates as is evident from different slopes in the edge shift curve associated to subsequent oxidation and reduction steps. Pulse shape and slope can be seen in the bottom part of Fig. 6. The reoxidation appears to be very rapid and the edge-shift curve shows a slope similar to that of the oxygen mass spectral signal. Rates as determined from the slope of the curves corresponding to normalized O_2 concentration and increasing MoO_3 content in the phase mixture upon oxidation (Fig. 6) are in the order of 1.0 min^{-1} (as calculated from the normalized phase content in Fig. 6 for comparison with the O_2 mass signal). Thus, the oxidation rate of the reduced MoO_{3-x} is determined by the O_2 pulse shape achievable in the *in situ* cell employed and does not appear to be limited by diffusion of O_2 into the MoO_{3-x} bulk. In contrast, the reduction with H_2 proceeds more slowly (in the order of 0.3 min^{-1}) during the time period in which the system is kept under a hydrogen atmosphere. Furthermore, an induction period of ~2 h in the isothermal reduction of bulk MoO_3 at 673 K was reported by Gajardo *et al.* (24). At 773 K a short induction period (~1 min) seems to be present as well (Fig. 4).

Differences in reduction/oxidation behavior of MoO_{3-x} obtained from AHM when compared to previous studies on the reduction of MoO_3 (6, 7, 31–33) indicate the influence of catalyst structure and preparation conditions on reactivity. Disorder and structural defects can considerably

accelerate reactions and, for instance, can prevent intermediates from being detected. A shift toward lower reduction temperatures in MoO_3 TPR studies (~800 to ~650 K) was observed for diluted samples (7) and small amounts of MoO_3 (6). However, the influence of structural defects was not elucidated. Furthermore, the observed rapid response of the entire MoO_{3-x} bulk to changes in the gas composition underlines the paramount importance of time-resolved *in situ* investigations in catalysis combined with suitable techniques to monitor catalyst performance. By no means can *ex situ* studies, which rely on diffusion limitations to freeze in particular states of a bulk sample (e.g., quenched and transferred catalyst), be expected to afford a representative image of the catalyst under reaction conditions.

Taking into account the rapid reaction of MoO_{3-x} during reactant pulses, it does not appear to be feasible to distinguish between surface and bulk reactions by means of pulse experiments. The assumption that structural responses in the system with time constants in the order of the reactant pulse correspond to surface reactions whereas a slow response indicates a bulk reaction evidently cannot be generalized. Hence, the value of pulse experiments to discern surface from bulk catalyzed reactions requires critical review. Instead *in situ* investigations capable of monitoring catalyst structure and catalytic performance with a sufficient time resolution have to be performed.

In order to determine the evolution of Mo valence during oxygen and hydrogen treatments and to identify molybdenum oxide phases present, a calibration curve was constructed from Mo K-edge shifts of MoO_2 and MoO_3 reference spectra (Fig. 7). Evaluation of the Mo K-edge position of the molybdenum oxide system during one reduction/oxidation cycle yielded an average valence of about 6 for the oxidized form and of about 5.4 for the reduced form. Apparently, this average valence lies between the average valence of Mo_4O_{11} and Mo_5O_{14}. Hence, solely based on the average valence it is difficult to distinguish between a mixture of MoO_3 and MoO_2, and the presence of well-defined molybdenum suboxides.

Based on the PCA analysis carried out no intermediate third phase was required to describe the experimental XANES spectra (Fig. 5). Instead a mixture of MoO_2 and MoO_3 was observed during reduction and oxidation which excludes the occurrence of structurally well-defined suboxides during reduction and reoxidation of MoO_3 at 773 K. Hence, results from the *in situ* investigation presented here are in agreement with the mechanism postulated by Arnoldy *et al.* (6). In order to illustrate structural changes necessary to transform a layered MoO_3 structure into the monoclinic MoO_2 structure, crystal structures of MoO_3 and MoO_2 are displayed in Fig. 13. Apparently, reduction of MoO_3 to MoO_2 requires considerable restructuring. On the one hand, given a certain amount of defects in the structure, intermediates may not be required for this transition. On the other hand, defects may speed up reduction and reoxidation to an extent that well-defined intermediate structures cannot be observed on the time scale employed. The latter cannot be excluded on the basis of the investigations described here. For the high-temperature

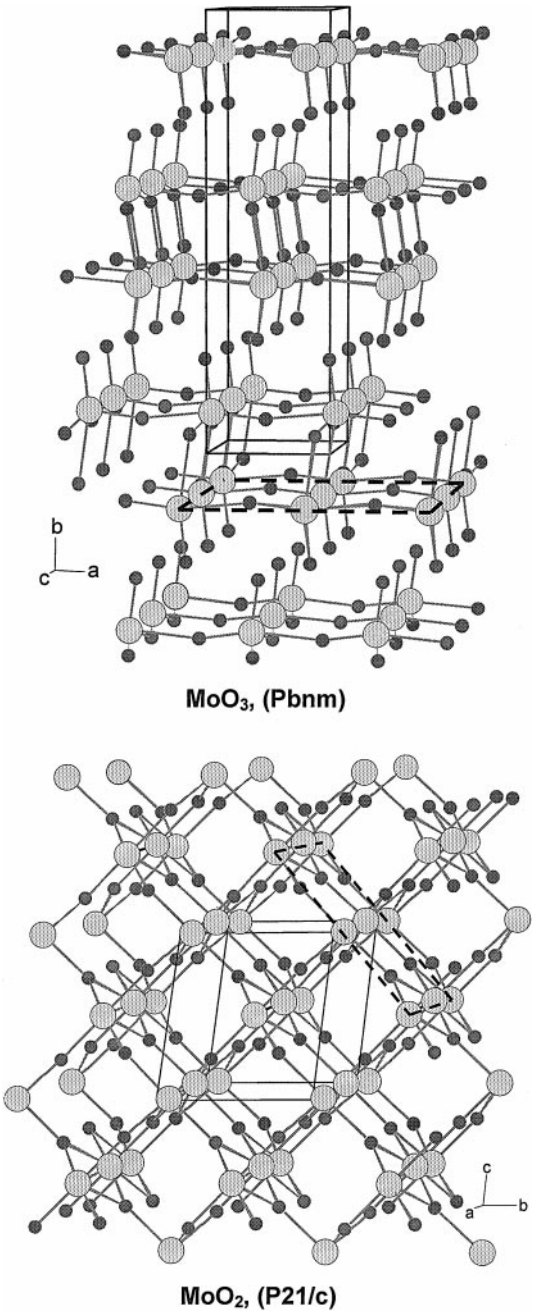

FIG. 13. Schematic representation of MoO_3 and MoO_2 crystal structures. Unit cells (solid) for each structure are indicated together with possible lattice planes (dashed) that may transform into each other upon reduction of MoO_3 to MoO_2. Orientation was chosen to emphasize parallel planes of MoO_6 units in both structures.

reduction of MoO_3 a rapid progress of the reaction was also found by Kuzmin *et al.* (32), in contrast to other results that postulated a two-step reduction mechanism ($MoO_3 \rightarrow Mo_4O_{11} \rightarrow MoO_2$) (33). However, the influence of catalyst pretreatment conditions has not been elucidated in previous studies and may have led to seemingly contradictory results regarding reaction intermediates. It becomes evident from the rates and phase composition reported here that pretreatment conditions and, hence, differences in bulk structure exhibit a considerable influence on reaction rates and the occurrence of intermediates and need to be properly taken into account.

EXAFS: Short- to Medium-Range Order

From the broadened *hkl* peak profiles of the top trace in Fig. 8 (inset) it can be seen that the decomposition of AHM resulted in a less crystalline and/or more disordered molybdenum oxide. However, no further evidence on the type of structural defects or the presence of molybdenum suboxides can be readily extracted from the XRD measurements.

Molybdenum trioxide possesses a number of structurally well-defined suboxides (Mo_nO_{3n-1}) where oxygen deficiency results in the occurrence of crystallographic sheer planes, in the structure (5, 34). Oxygen deficiency in these structures is accommodated by sheer planes resulting in corner-shared (CS) and edge-shared (ES) coordination of neighboring MoO_6 octahedra in contrast to a regular layered structure with a nominal stoichiometry of MoO_3 which would have only corner-shared octahedra. Based on a simplified structural model for Mo_8O_{23} (34), theoretical EXAFS phases and amplitudes were calculated utilizing the FEFF code. Afterward, the most prominent single-scattering paths in the structure (i.e., Mo–O and edge- and corner-shared Mo–Mo) were employed in an EXAFS refinement to the experimental MoO_{3-x} FT($\chi(k)$) (Fig. 9). Figure 14 shows magnitude and imaginary part of the resulting theoretical EXAFS function together with the experimental FT($\chi(k)$). A reasonably good agreement in the imaginary part indicates the validity of a structural model possessing corner-shared and edge-shared octahedra. The poor match in amplitude, in particular at about 2.5 Å, is caused by a strong contribution of multiple-scattering paths in this region that were not included in the refinement.

Numerous studies in catalysis have related catalyst activity and selectivity to the presence of certain defects in the structure; therefore, knowledge about the presence of defects and their correlation to catalytic performance is of paramount importance for a complete understanding of the catalyst. Apparently, structural defects (i.e., edge-shared octahedra) observed *in situ* in MoO_{3-x} (Fig. 9) were not readily detectable with X-ray diffraction (Fig. 8). Hence, defects seem to be randomly distributed in the MoO_{3-x}

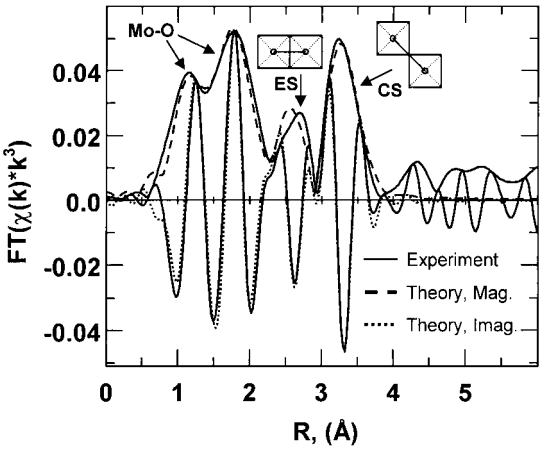

FIG. 14. Experimental and theoretical Fourier transformed $\chi(k)$ of MoO_{3-x} obtained from AHM decomposition. Theoretical phases and amplitudes calculated for the simplified suboxide structure (Mo_8O_{23} (34)) were used in the refinement.

structure, rather than exhibit a long-range ordered sheer structure. Rapid reduction and reoxidation observed in this work are probably related to this disordered MoO_{3-x} structure. Detailed investigations of structural defects (such as sheer planes and the ratio of edge-shared to corner-shared octahedra) of molybdenum oxide systems under various reaction conditions will be the subject of future *in situ* TR-XAS investigations.

Oscillatory Behavior in Propene Oxidation

Bistability regions and chemical oscillations far from thermodynamical equilibrium are well-known phenomena on noble metals and have been studied extensively in the past. However, much less is known about oscillatory behavior in oxidation reactions on metal oxides at elevated temperature and atmospheric pressure. Amariglio *et al.* reported an oscillating oxidation of propene on copper oxides (35). However, structural changes were deduced only from visual inspection of the catalyst *in situ* and *ex situ* XRD measurements. A recent review on the field of dynamic behavior and bistabilities in heterogeneous catalysis is given by Slin'ko and Jaeger (36). Here we present for the first time dynamic behavior of the bulk structure of a metal oxide under reaction conditions measured *in situ* by time-resolved X-ray absorption spectroscopy. Oscillating alterations in the Mo K-edge XANES were observed during reduction of MoO_{3-x} with propene at 773 K (Fig. 12). However, no periodic oscillations were found in mass spectra of the gas phase measured during the reaction (reaction products detected were carbon dioxide, water, and trace amounts of propenal). Instead, we found irregular oscillations that did not exhibit a fixed relationship to the observed dynamic behavior in the XANES spectra. Further investigations and a detailed EXAFS analysis of the described phenomenon

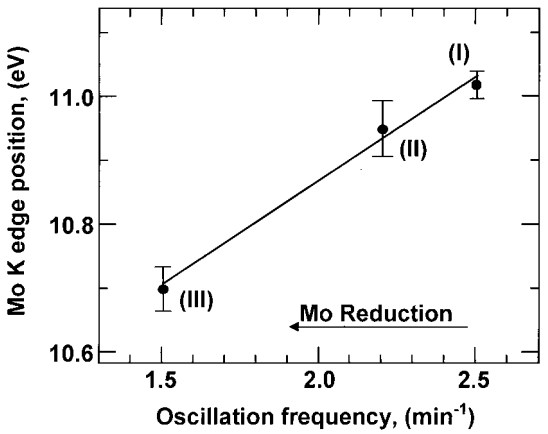

FIG. 15. Linear relationship between Mo 1*s*–4*d* pre-edge peak height oscillation frequency (Fig. 14) and Mo K-edge position (valence). The frequencies correspond to the regions I–III in Fig. 14 and were obtained from a Fourier analysis of the periodic oscillations.

are intended for the nearest future and shall further elucidate the mechanism of the observed dynamic behavior in the selective propene oxidation on MoO_{3-x}.

The evident correlation between external perturbation (H_2 pulses) and alterations in the electronic and geometric structure of the molybdenum oxide system (Fig. 12) excludes the possibility of experimental artifacts being responsible for the described oscillatory behavior. Dynamic changes were found only in the pre-edge peak height. The Mo K-edge position did not exhibit a periodic shift but only a continuous decrease toward lower photon energy, i.e., a "slow" reduction of the molybdenum oxide during H_2 pulses. Continuous reduction of molybdenum oxide with time is also consistent with the overall decrease of the 1*s*–4*d* peak height in Fig. 12. Periodic oscillations in pre-edge peak height seem to be superimposed to this continuous decrease. Interestingly, from a Fourier analysis of the corresponding pre-edge peak height data for the different regions in Fig. 12 a linear dependence of the oscillation frequency on the Mo valence (Fig. 15) was found.

In Fig. 11 XANES spectra of as-purchased MoO_2 and MoO_3 are depicted. The spectrum of MoO_3 exhibits a pre-edge peak, which is attributed to an inner-atomic 1*s*–4*d* transition (37), whereas only an extremely weak structure can be seen at the same photon energy in the second derivative of the spectrum of MoO_2. The MoO_3 pre-edge peak indicates the presence of strongly distorted MoO_6 octahedra in the MoO_3 structure (Fig. 10), resulting in a mixing of oxygen 2*p* orbitals with 5*p* and 4*d* orbitals of molybdenum (38). This mixing enables a dipole-allowed transition into unoccupied molecular orbitals and, hence, a much stronger pre-edge signal than the quadrupole-allowed 1*s*–4*d* transition in a regular MoO_6 octahedron.

From the observed periodic oscillations in the Mo 1*s*–4*d* pre-edge peak height (Fig. 12) we therefore conclude that this dynamic behavior is not related to an oscillating oxidation–reduction of Mo but rather indicates an oscillating alteration in the degree of distortion of MoO_6 octahedra in the structure. A continuous reduction of molybdenum is caused by hydrogen pulses and the ongoing oxidation of propene. The oscillating alterations in the molybdenum oxide structure during propene oxidation may constitute first experimental evidence for dynamic bulk structural changes during oxygen transport and replenishing of surface oxygen from the MoO_{3-x} bulk.

CONCLUSION

The bulk structure of molybdenum oxide (MoO_{3-x} obtained from AHM decomposition) under rapidly changing reaction conditions was investigated *in situ* with TR-XAS at the Mo K-edge. Oxygen and hydrogen pulse experiments at 773 K yielded a swift response of the MoO_{3-x} bulk structure to changes in the reactant composition. Observed rates were in the same order as reactant pulses which excludes bulk diffusion limitations on the time scale employed (<1 min). The Mo valence of the oxidized and the reduced phase of one reduction–oxidation cycle was determined to be $\leq$6.0 and $\sim$5.4, respectively. Principal component analysis (factor analysis) of Mo K-edge XANES spectra identified two constituent phases during reduction and reoxidation, namely MoO_2 and MoO_3. EXAFS analysis revealed an edge-shared octahedral coordination in the molybdenum oxide structure presumably due to the presence of sheer-plane-like defects. Furthermore, for the first time, chemical oscillations in the propene oxidation on MoO_{3-x} at 773 K were measured by *in situ* TR-XAS. The periodic behavior observed in the Mo K-near-edge indicates dynamic bulk structural changes during oxygen transport and replenishing of surface oxygen from the MoO_{3-x} bulk. Hydrogen pulses were found to perturb the periodic oscillations with the oscillation frequency exhibiting a linear dependence on the Mo valence.

The work reported herein clearly demonstrates the suitability of time-resolved energy-dispersive XAS experiments for bulk structural *in situ* investigations of heterogeneous catalysts. The rapid bulk structural changes observed during pulse experiments underlines the importance of *in situ* experiments, since relying on bulk diffusion limitations for *ex situ* investigations seems to be restricted to special applications. Also, a critical review of the ability of pulse experiments to distinguish between surface and bulk reactions appears to be necessary. Moreover, it is evident from the work reported here that continuously monitoring the reactant composition on a sufficiently small time scale during *in situ* experiments is an imperative prerequisite if bulk structure modifications are to be correlated to catalytic performance. In future experiments we intend to complement time-resolved energy-dispersive experiments with conventional XAS investigations under steady-state

conditions. On the one hand, subsecond-range experiments shall elucidate kinetic and mechanism of the dynamic behavior of transition metal oxides under selective oxidation conditions. Conventional XAS experiments, on the other hand, will afford reliable structural information that can be combined with results from complementary bulk and surface analysis techniques.

ACKNOWLEDGMENTS

We acknowledge the European Synchrotron Radiation Facility (ESRF) for providing beamtime for this work. Assistance of the ID24 staff during the experiments is also gratefully acknowledged. T.R. wishes to thank the Deutsche Forschungsgemeinschaft, DFG, for financial support (Habilitationsstipendium).

REFERENCES

1. Grasselli, R. K., *Catal. Today* **49**, 141 (1999).
2. Bettahar, M. M., Costentin, G., Savary, L., and Lavalley, J. C., *Appl. Cat. A* **145**, 1 (1996).
3. Haber, J., and Lalik, E., *Catal. Today* **33**, 119 (1997).
4. Mars, P., and van Krevelen, D. W., *Chem. Ing. Sci.* **3**, 41 (1954).
5. Barber, S., Booth, J., Pyke, D. R., Reid, R., and Tilley, J. D., *J. Catal.* **77**, 180 (1982).
6. Arnoldy, P., de Jonge, J. C. M., and Moulijn, J. A., *J. Phys. Chem.* **89**, 4517 (1985).
7. Regalbuto, J. R., and Ha, J. W., *Catal. Lett.* **29**, 189 (1994).
8. Aritani, H., Tanaka, T., Funabiki, T., Yoshida, S., Kudo, M., and Hasegawa, S., *J. Phys. Chem. B* **100**, 5440 (1996).
9. Han, Y. H., Ueda, W., and Moro-Oka, Y., *Appl. Catal. A* **176**, 11 (1999).
10. Schlögl, R., *Angew. Chem. Int. Ed.* **32**, 381 (1993).
11. Bearden, J. A., and Burr, A. F., *Rev. Mod. Phys.* **39**, 125 (1967).
12. Hagelstein, M., San Miguel, A., Fontaine, A., and Goulon, J., *J. Phys. IV* **7**, C2-C303 (1997).
13. Hagelstein, M., Ferrero, C., Hatje, U., Ressler, T., and Metz, W., *J. Synch. Rad.* **2**, 174 (1995).
14. Ressler, T., *J. Phys. IV* **7**, C2-C269 (1997).
15. Ressler, T., Hagelstein, M., Hatje, U., and Metz, W., *J. Phys. Chem. B* **101**, 6680 (1997).
16. Ressler, T., *J. Synch. Rad.* **5**, 118 (1998).
17. Koningsberger, D. C., and Prins, R., "X-ray Absorption Spectroscopy, Chemical Analysis," 92. Wiley, New York, 1988.
18. Rehr, J. J., Booth, C. H., Bridges, F., and Zabinsky, S. I., *Phys. Rev. B* **49**, 12347 (1994).
19. Rehr, J. J., Albers, R. C., and Zabinsky, S. I., *Phys. Rev. Lett.* **69**, 3397 (1992).
20. Soldatov, A. V., Ivanchenko, T. S., Stekhin, I. E., Bianconi, A., and Ingalls, R., *Phys. Status Solidi B* **184**, 237 (1994).
21. Ressler, T., Brock, S. L., Wong, J., and Suib, S. L., *J. Phys. Chem. B* **103**, 6407 (1999).
22. Wyckoff, W. G., "Crystal Structures," Bd. 1-3. Interscience, New York, 1965.
23. Bolzan, A. A., Kenned, B. J., and Howard, C. J., *Austr. J. Chem.* **48**, 1473 (1995).
24. Gajardo, P., Grange, P., and Delmon, B., *J. Chem. Soc. Faraday Trans. I* **76**, 929 (1980).
25. Ratnasamy, P., *et al.*, *J. Catal.* **38**, 19 (1975).
26. Batist, Ph. A., *et al.*, *J. Catal.* **7**, 33 (1967).
27. Malinowski, E. R., and Howery, D. G., "Factor Analysis in Chemistry." Wiley, New York, 1980.
28. Ressler, T., Wong, J., Roos, J., and Smith, I. L., *Environ. Sci. Tech.* (in press).
29. Günter, M. M., Herein, D., Schumacher, R., Weinberg, G., and Schlögl, R., *J. Vac. Sci. Technol. A* **16**, 3526 (1998).
30. Kihlborg, L., *Ark. Kemi* **21**, 357 (1963).
31. Carpenter, K. H., and Hallada, C. J., "Proceedings, 3rd International Conference on Chemistry and Uses of Molybdenum." Climax Molybdenum, London, 1979.
32. Kuzmin, A., Purans, J., Parent, P., and Dexpert, H., *J. Phys. IV* **7**, C2-C891 (1997).
33. Sloczynski, J., *J. Solid State Chem.* **118**, 84 (1995).
34. Cotton, F. A., and Wilkinson, G., *Advanced Inorganic Chemistry*, 4th Ed. Wiley, New York, 1982.
35. Amariglio, A., Benali, O., and Amariglio, H., *J. Catal.* **118**, 164 (1989).
36. Slin'ko, M. M., and Jaeger, N. I., "Oscillating Heterogeneous Catalytic Systems." Elsevier, Amsterdam, 1994.
37. Cramer, S. P., Hodgson, K. O., Gillum, W. O., and Mortenson, L. E., *J. Am. Chem. Soc.* **100**, 3398 (1978).
38. Tullius, T. D., Gillum, W. O., Carlson, R. M., and Hodgson, K. O., *J. Am. Chem. Soc.* **102**, 5670 (1980).